arXiv:1605.03442v3 [cond-mat.mtrl-sci] 19 Apr 2017

Anomalous temperature dependence of the band-gap in Black Phosphorus

Cesar E. P. Villegas,[*,†,‡] A. R. Rocha,[‡] and Andrea Marini[†,¶]

Istituto di Struttura della Materia of the National Research Council, Via Salaria Km 29.3,I-00016 Monterotondo Stazione, Italy., Instituto de Física Teórica, Universidade Estadual Paulista (UNESP), Rua Dr. Bento T. Ferraz, 271, São Paulo, SP 01140-070, Brazil., and European Theoretical Spectroscopy Facilities (ETSF)

E-mail: villegas@ift.unesp.br

Abstract

Black Phosphorus (BP) has gained renewed attention due to its singular anisotropic electronic and optical properties that might be exploited for a wide range of technological applications. In this respect, the thermal properties are particularly important both to predict its room temperature operation and to determine its thermoelectric potential. From this point of view, one of the most spectacular and poorly understood phenomena is, indeed, the BP temperature–induced band–gap opening: when temperature is increased the fundamental band–gap increases instead of decreasing. This anomalous thermal dependence has also been observed, recently, in its monolayer counterpart. In this work, based on *ab-initio* calculations, we present an explanation

[*]To whom correspondence should be addressed

[†]Istituto di Struttura della Materia of the National Research Council, Via Salaria Km 29.3,I-00016 Monterotondo Stazione, Italy.

[‡]Instituto de Física Teórica, Universidade Estadual Paulista (UNESP), Rua Dr. Bento T. Ferraz, 271, São Paulo, SP 01140-070, Brazil.

[¶]European Theoretical Spectroscopy Facilities (ETSF)

for this long known, and yet not fully explained, effect. We show that it arises from a combination of harmonic and lattice thermal expansion contributions, which are, in fact, highly interwined. We clearly narrow down the mechanisms that cause this gap opening by identifying the peculiar atomic vibrations that drive the anomaly. The final picture we give explains both the BP anomalous band–gap opening and the frequency increase with increasing volume (tension effect).

Keywords: electron-phonon, thermal expansion, black phosphorus, gap temperature dependence, temperature coefficient, MBPT

Recently, black phosphorus (BP), a layered puckered structure of P atoms has gained renewed attention due to its remarkable anisotropic optical,[1] electrical[2,3] and thermal properties.[4] In contrast to other layered semiconductors, the band gap in BP can be adjusted from 0.33 to 2.0 eV depending on the number of layers.[5] Due to these peculiar properties, it has been rapidly envisioned the possibility of integrating BP for several technological applications.[6,7] In fact, recent reports have indicated that BP and its monolayer counterpart hold great potential for designing thermoelectric devices as their figure of merit can go from 0.7 to 2.5 under controlled doping and temperature conditions.[8,9] These findings have highlighted questions regarding the origin of such high thermoelectric performance and, most importantly, the fundamental role played by temperature.

The band gap temperature dependence in semiconductors is a well understood phenomena for a large group of materials, for which one observes a monotonic decrease of the energy gap as temperature increases.[10,11] Nevertheless, there are some exceptional materials that exhibit an anomalous temperature dependence: the gap increases instead of decreasing. Two kinds of anomalies are known: non-monotonic and monotonic. In the first case, the gap increases at low temperatures and decreases for high temperatures.[12,13] In the second case, instead, the gap continuously increases with temperature. This is the case of some perovskites,[14] Copper halides[15] and lead chalcogenides.[16,17] Despite the abundance of exper-

imental evidence, and theoretical results based on different approaches[17–19] and models,[20,21] fully *ab-initio* theoretical studies addressing the origin of the anomalous gap dependence are still scarce.

Some clear experimental evidences,[22,23] recently confirmed by the photoluminescence spectrum of its monolayer counterpart,[24] have indicated that BP follows a monotonic increase of the band-gap. This trend has been explained neither theoretically nor experimentally. Indeed most vibrational studies performed on BP have characterized the phonon modes[25,26] and investigated the phonon thermal transport.[4,8,9] Consequently, the role of the electron-phonon interaction[27] and lattice expansion in black phosphorus are, so far, poorly understood.

In this work, we provide a comprehensive description of the anomalous band gap temperature dependence of black phosphorus. By using *ab-initio* calculations, we study both the harmonic (electron-phonon coupling) and lattice thermal expansion (variable volume) contributions. For the harmonic part, the mechanism is driven by the coupling between electronic states with acoustic modes and the transverse optical mode B_{1u}. The coupling stems from long-range amplitude vibrations that are favored by the particular puckered crystal structure. For the lattice thermal expansion (LTE) term the anomaly arises due to the BP negative pressure coefficient. We also show that BP volume expansion induces a tension effect[28] via transverse optical vibrations. Our results show an excellent agreement with experimental $E_g(T)$ curves slope and emphasizes the crucial role of both harmonic and LTE contributions.

In the finite temperature regime, the temperature (T) dependence of the single particle state energy is $E_{n\mathbf{k}}(T) = \epsilon_{n\mathbf{k}} + \Delta E_{n\mathbf{k}}(T)$, with $n\mathbf{k}$ the level index and $\epsilon_{n\mathbf{k}}$ the energy in the case where all atoms are kept frozen in their equilibrium position and treated classically. $\Delta E_{n\mathbf{k}}(T)$ comprises two contributions for temperatures below the Debye temperature (Θ_D)[29]

$$\Delta E_{n\mathbf{k}}(T) \approx \Delta E_{n\mathbf{k}}(T)\big|_{har} + \Delta E(T)\big|_{LTE}. \tag{1}$$

The first term represents harmonic (constant volume) contributions induced by the pure electron-phonon interaction. This includes explicitly the temperature dependence through the Bose-Einstein occupation function of the phonon modes, as explained in the Methods section. The second term describes the LTE (variable volume) effects,

$$\Delta E(T)\big|_{LTE} = -\frac{1}{\chi}\frac{\partial E_g}{\partial P}\Big|_T \int_0^T \beta(T')dT'. \tag{2}$$

In Eq (2), β and χ are the volumetric thermal expansion coefficient and compressibility, respectively. Considering the anisotropic crystal structure of BP, the volumetric coefficient is calculated as $\beta{=}\alpha_a{+}\alpha_b{+}\alpha_c$, where α_i is the linear expansion coefficient along the crystallographic directions shown in Fig. (1-a). Eq. (1) includes the so-called zero point motion (ZPM) effect[10,30] ($\Delta E_{n\mathbf{k}}(T \to 0)$) which is typically non-zero due to the quantum nature of the atoms.

Moreover, from Eq. (1) it is clear that the harmonic and LTE terms must be treated on equal footing. Nevertheless their relative strength strongly depends on the material. In simple semiconductors with a standard monotonically decreasing gap dependence we have that, generally, $\Delta E(T)\big|_{LTE} \ll \Delta E_{n\mathbf{k}}(T)\big|_{har}$. In systems with an anomalous trend, instead, the role played by the two contributions turn out to be of the same order of magnitude.[18,19] The case of PbTe, probably the most well studied lead chalcogenide, is exemplar. PbTe shows a clear band-gap anomaly of the second kind. This has been interpreted in terms of both strong anharmonic[31,32] and harmonic[17–19] effects, but to date, fully *ab-initio* studies including retardation effects are not available to support this picture. This example demonstrates that a clear atomistic interpretation of the elemental mechanism that drives the anomaly is still missing. In this work, instead, we will unambiguously identify the specific atomic oscillations responsible for the anomalous gap dependence using a fully *ab-initio* approach.

In our calculations the electron-phonon interaction is treated within the *ab-initio* Many-Body Perturbation Theory (MBPT) framework.[33,34] In MBPT the electron-phonon coupling

is composed by a first and second order Taylor expansion in the nuclear displacement, fully including retardation effects caused by the different electronic and phononic dynamics. The LTE contribution is calculated by using first principles within the quasiharmonic approximation (QHA).[35] See Methods section for details.

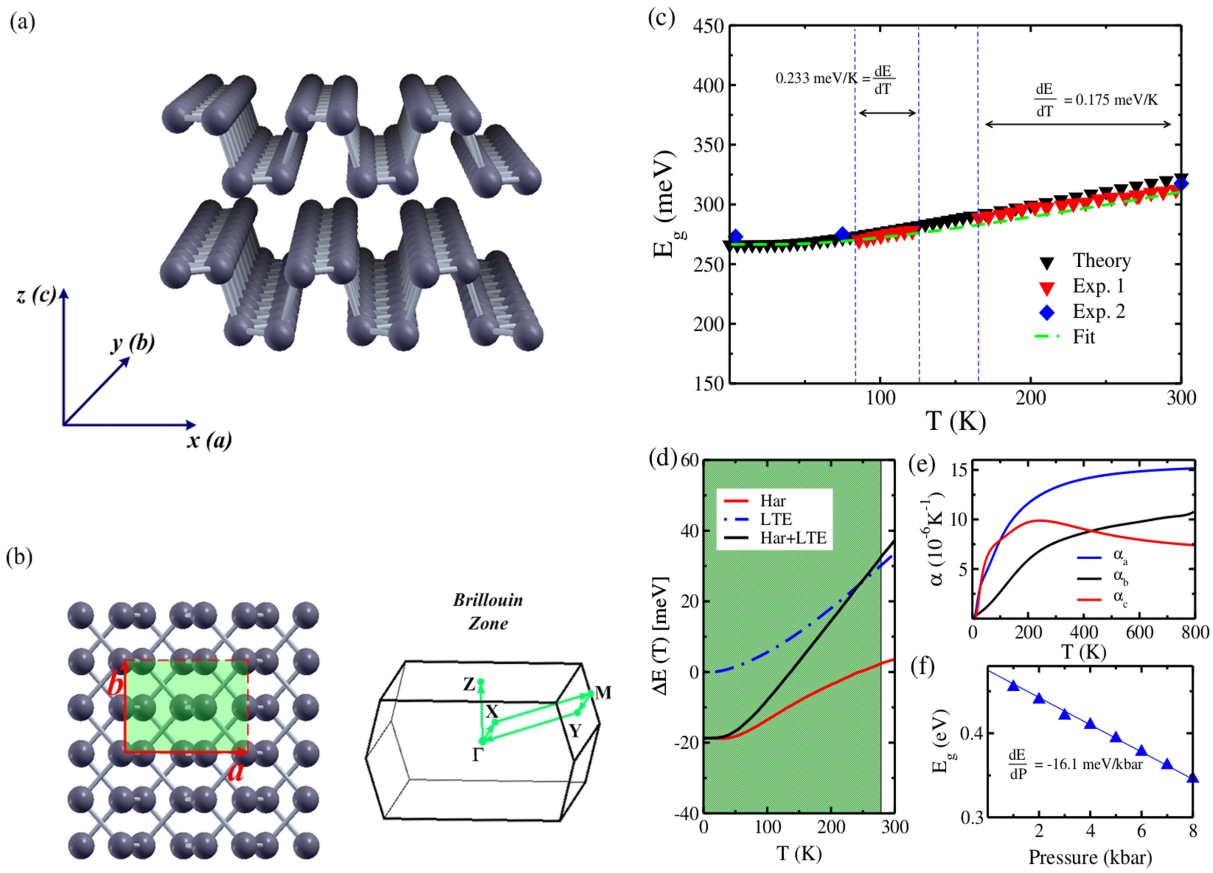

Figure 1: (a-b) Schematic representation of the atomic structure and Brillouin zone of Black Phosphorus showing the main crystallographic directions. (c) Theoretical and experimental BP band-gap thermal dependence split in frame (d) in harmonic and LTE contributions obtained from *ab-initio* MBPT and the QHA, respectively. The relevant thermodynamic observables required for computing the LTE term such as (e) the linear expansion coefficients along the different crystal directions and (f) the energy gap change as a function of pressure, obtained from DFT, are also shown. Green dashed-line in (c) is a fit with a three oscillator Bose-Einstein model for frequencies 136, 195 and, 450 cm^{-1} which represent the most intense peaks in the experimental BP phonon density of states.[36] The green shaded region indicates the temperature range below 282K.

In Fig. (1-c) we show the BP band gap measurements[22,23] as a function of temperature compared to our theoretical results. One can clearly observe the monotonic increase of the ex-

perimental band gap nicely described by our calculations. The size of $\Delta E_g(T)$–$\Delta E_g(T \to 0)$ can be as large as 50 meV at room temperature. For low-temperatures, we obtain an excellent agreement with the experimental slope while, as the temperature increases, the theoretical result slightly deviates from the experimental one. Our interpretation of this deviation is based on the observation that as T increases $\Delta E(T)\big|_{LTE}$ rapidly becomes dominant. This points to the importance of anharmonic corrections that, however, in Eq. (1) are not fully introduced. Thus we ascribe the high temperature deviation to the missing anharmonic corrections to the electron-phonon and thermal expansion terms.

From the harmonic contribution shown in Fig. (1-d), we estimate a value of -18.3±0.9 meV for the ZPM correction. This is comparable with those reported in other narrow band gap materials.[10] In addition, we observe that the positive slope of the harmonic term smoothly decreases beyond 180K. In contrast, the LTE correction increases continuously reaching values as large as 33 mev at room temperature. Note that in Fig. (1-c), the value ϵ_g=282.7 meV was added to the sum of the harmonic and LTE contributions to match the $E_g(T \to 0)$ obtained from the fitted curve using Einstein's model, the green-dashed curve in Fig. (1-c). This rigid shift does not affect our conclusions as the main goal of this work is the description of the slope of $E_g(T)$, and not the absolute values of the band-gap. This is done in order to avoid the discrepancies observed in describing the BP band-gap at different theory levels.[5,37]

The linear expansion and pressure coefficients of BP are shown in Figs (1-e) and (1-f). These thermodynamic observables, together with the experimental value for the compressibility,[38] ($\chi = 3.02 \times 10^{-3}$ kbar^{-1}) were used to compute $\Delta E(T)\big|_{LTE}$ in Eq. (2). The linear expansion coefficients reflect the anisotropic character of the BP crystal as they are different for each crystallographic direction. The 800K scale is covered in order to show their trend. For completeness, the lattice parameters as a function of temperature are presented in the Supporting Information. In addition, from Fig. (1-f), we observe that the effect of pressure is to significantly reduce the band gap of the crystal. By performing a linear fit of the $E_g(P)$

Table 1: Temperature slopes dE_g/dT for different temperature ranges obtained by performing a linear fit of $E_g\,(T)$.

Temperature Coefficient (meV/K)				
	Harmonic	LTE	Total	Experiment [22]
$\frac{\Delta E_g}{\Delta T}\big\|_{80<T<120K}$	0.100	0.99	0.199	0.233
$\frac{\Delta E_g}{\Delta T}\big\|_{160<T<300K}$	0.085	0.150	0.235	0.175

data, we estimate a negative pressure coefficient of ≈ -16.1 meV/kbar, which is in excellent agreement with the experimental value of, -16.4 meV/kbar.[23,39] It should be noticed that the positive slope observed in the LTE term is a direct consequence of the negative pressure coefficient as $\Delta E(T)\big|_{LTE} \propto -\frac{\partial E_g}{\partial P}$.

The $E_g(T)$ slopes for different temperature ranges are summarized in table 1. The results show that the harmonic term is responsible for roughly 50 % of the total contribution for temperatures up to 160K. However as the temperature increases (T>160K), the electron-phonon contribution gets weaker, with a slope ≈ 0.085 meV/K, indicating that the LTE contribution becomes the dominant one.

The correct description of the experimental $E_g(T)$ curve is one of the key result of this work. In addition, the use of an *ab-initio* approach allow us to further investigate the elemental mechanism that drives the BP gap anomaly.

1 Discussion

To elucidate the origin of the anomalous thermal behaviour we first analyze the LTE (volume variable) contribution. For this purpose, we compute the Grüneisen parameters

$$\gamma_{\mathbf{q}\lambda} = -\frac{\partial \ln \omega_{\mathbf{q}\lambda}}{\partial \ln V}, \tag{3}$$

which allows us to quantify the anharmonicity associated to a given phonon mode λ. In Fig. (2-a) the Grüneisen parameters for low-frequency optical modes are presented. We clearly

observe that the $\gamma_{\mathbf{q}\lambda}$ of transverse optical (TO) mode B_{1u} shows a strong negative intensity around the Γ point, becoming the most anharmonic optical mode at the center of the Brillouin zone (BZ) (see also Fig. 2-b). From Eq. (3), it follows that negative values of γ induces an increase of the phonon frequency as the system's volume expands, contrary to the usual behaviour. This is a well known thermal mechanism, observed also in some vibrational modes of graphene and graphite,[40] that lead them to a negative volumetric thermal expansion.[41] Taking a closer view on the vibrational mechanism of mode B_{1u} depicted in Fig. (2-d), we argue that this particular negative $\gamma_{\mathbf{q}\lambda}$ is a direct consequence of the puckered crystalline structure. Indeed, during a volumetric expansion, the force constant as well as the frequencies of in-plane bonds are reduced. Simultaneously, superficial potential energy is gained due to the tension produced among bonds. Thus, the induced in-plane tension will cause a frequency increase for the atoms vibrating transversally, like in the B_{1u} mode. This is referred in literature as tension effect[28] and it is analogous to stretching a string and applying a transversal force which results in higher frequency vibrations.

In contrast to the transverse optical modes (B_{1u} and B^2_{3g}), longitudinal and out-of-plane optical modes shown in Fig. (2-b), present positive values for γ_λ at the center of the BZ, reflecting the usual reduction of their frequencies as the material expands. Overall, the dispersion of the Grüneisen parameters reflects the structural anisotropy of the material.

For completeness, in Fig. (2-c), we present the Grüneisen parameter as a function of the phonon frequencies. As expected, we observe strong anharmonicity in the acoustic modes as they play a crucial role in umklapp scattering processes. Most importantly, within the frequency range from 100-175 cm^{-1}, depicted as a grey-shadow region, we observe thermal anomalies (negative value of γ_λ) for optical as well as acoustic modes. As these modes are crucial for both harmonic and LTE terms of the anomalous gap dependence, we refer to the highlighted grey region of Fig. (2-c) as anomalous region (AR). The B_{1u} mode falls in this range. In order to understand the vibrational mechanisms in this region, in Figs. (2 e-h) we plot the superficial phonon potential for modes transverse acoustic (TA), longitudinal

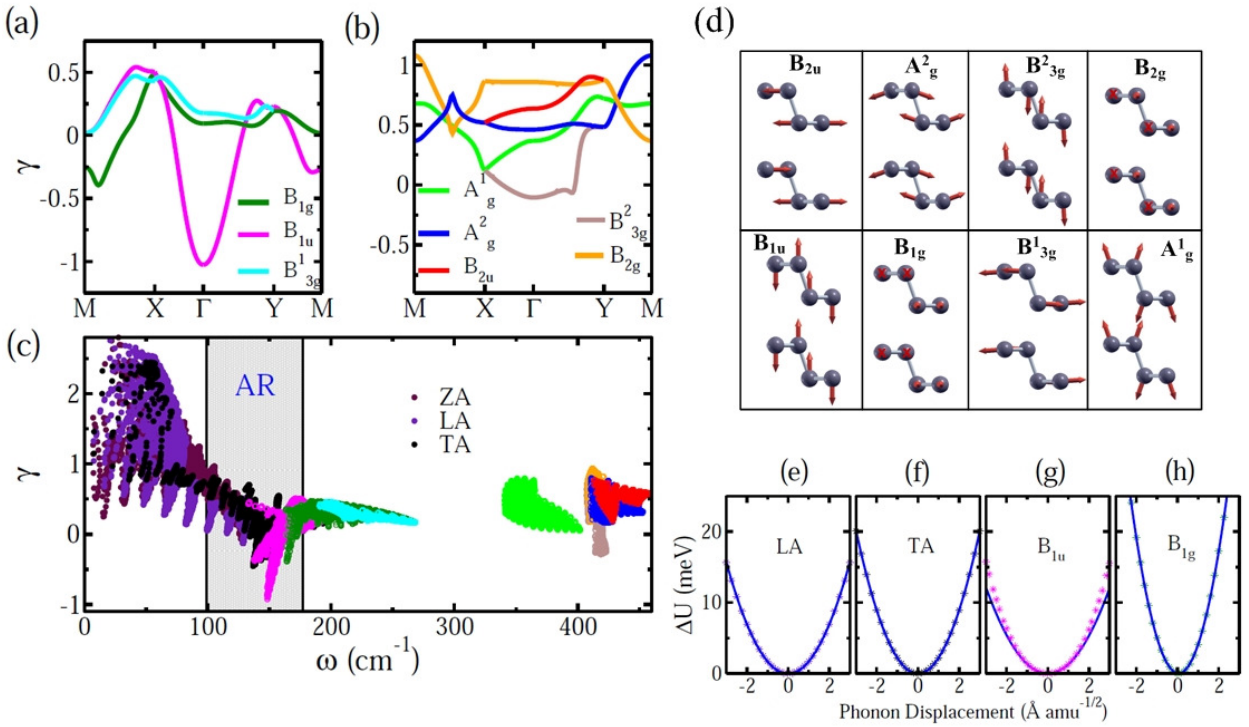

Figure 2: Variable volume (LTE) behaviour of the phonon modes in BP studied within the QHA. The Grüneisen parameters are shown along the $MX\Gamma YM$ path for: (a) low-frequency and (b) high frequency optical modes. (c) Grüneisen parameters mapped on the whole Brillouin zone. The anomalous region (AR) is represented with grey-shadow color. (d) Schematic representation of phonon vibrations in BP. (e-h) Superficial potential energy profile for LA, TA, B_{1u} and B_{1g} modes. For the acoustic modes the potential is obtained at the M point, whereas the Γ point is used for the optical modes. Solid blue lines represent a parabolic fit.

acoustic (LA), B_{1u} and B_{1g}. Large phonon amplitudes around the equilibrium position is observed for modes LA, TA, and B_{1u}. This reveals the easiness of these modes to be scattered when coupled with electrons. In contrast, the small phonon displacements found in mode B_{1g} remarks it robustness to be scattered. In addition, as the B_{1u} phonon amplitude increases, anharmonic features appear. This is observed by fitting an harmonic potential (parabola), indicated by the blue-solid line in Fig. (2 e-h).

The link between the negative Grüneisen parameters, the anomalous gap dependence and a family of specific modes may appear fortuitous. Instead these modes, belonging to the AR, are the only driving force of the entire and peculiar thermal behaviour of BP.

Indeed, in order to investigate the phonon mode contributions to $\Delta E_g(T)\big|_{har}$, we intro-

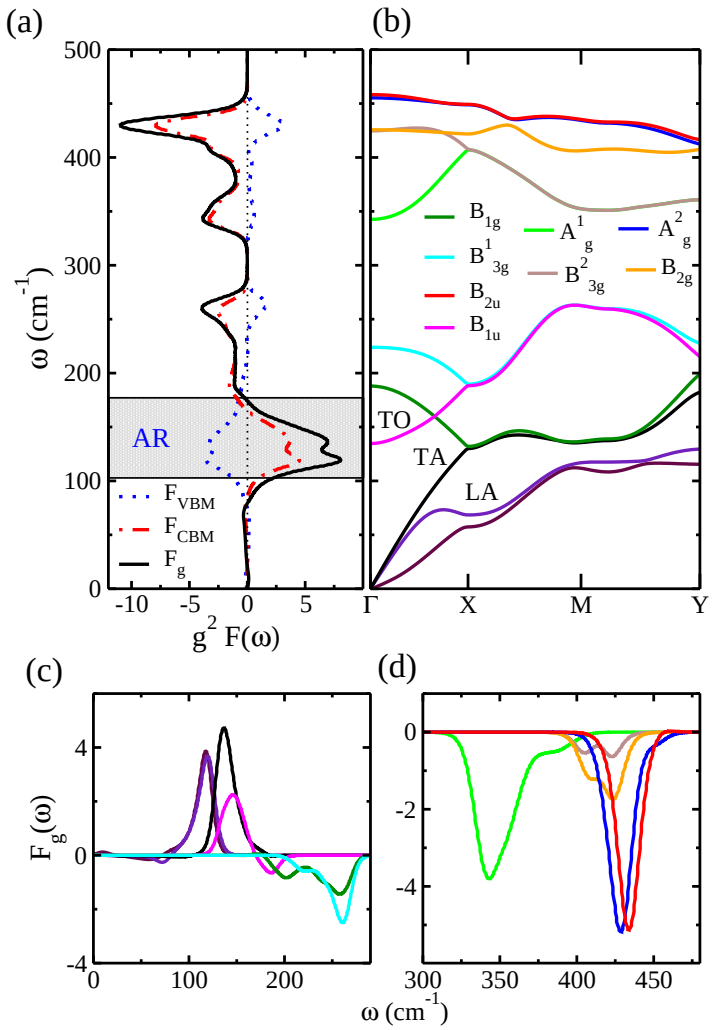

Figure 3: Constant volume (harmonic) behaviour of BP phonon modes studied within MBPT. (a) Electron-phonon spectral function for VBM (blue dotted-line), CBM (red dot-dashed line) and band-edge (black solid line). As $\Delta E_g(T)\big|_{har} \propto \int d\omega g^2 F_g(\omega)[N_{\mathbf{q}\lambda}(\omega,T)+1/2]$, the positive g^2F_g region corresponds to a temperature increasing $E_g(T)$. As in the LTE part the modes of the AR drive the anomaly (gray-shadow region). (b) BP phonon dispersion along the ΓXMY path and band edge Eliashberg spectral function projected on phonon modes with frequencies (c) bellow 300 cm^{-1} and (d) above 300 cm^{-1}.

duce the generalized Eliashberg function

$$g^2F_{n\mathbf{k}}(\omega) = \sum_{n'\mathbf{q}\lambda} \Big[\frac{|g^{\mathbf{q}\lambda}_{nn'\mathbf{k}}|^2}{\epsilon_{n\mathbf{k}} - \epsilon_{n'\mathbf{k-q}}} - \frac{1}{2}\frac{\Lambda^{\mathbf{q}\lambda}_{nn'\mathbf{k}}}{\epsilon_{n\mathbf{k}} - \epsilon_{n'\mathbf{k}}}\Big]\delta(\omega - \omega_{\mathbf{q}\lambda}). \tag{4}$$

This function is defined within the adiabatic limit which corresponds to the condition $|\epsilon_{n\mathbf{k}} - \epsilon_{n'\mathbf{k-q}}| \gg \omega_{\mathbf{q}\lambda}$. In this work we use the fully dynamical description for $\Delta E_{n\mathbf{k}}(T)\big|_{har}$ (see Methods section). Nevertheless, the adiabatic $g^2F_{n\mathbf{k}}(\omega)$ provides useful insights into the decomposition and physical understanding of the temperature dependence of the electronic states as it defines the adiabatic contribution to $\Delta E_{n\mathbf{k}}(T)\big|_{har}$ as

$$\Delta E_{n\mathbf{k}}(T)\big|^{adiab}_{har} \approx \int d\omega g^2F_{n\mathbf{k}}(\omega)[N_{\mathbf{q}\lambda}(\omega, T) + \frac{1}{2}]. \tag{5}$$

Dynamical corrections are defined in Eq. (10). In Eq. (5), $N_{\mathbf{q}\lambda}(\omega, T)$ is the Bose-Einstein distribution while in Eq. (4), $\omega_{\mathbf{q}\lambda}$ are the phonon frequencies and $g^{\mathbf{q}\lambda}_{nn'\mathbf{k}}$ and $\Lambda^{\mathbf{q}\lambda}_{nn'\mathbf{k}}$ are the first and second-order electron-phonon matrix elements, which are related to the Fan and Debye-Waller (DW) contributions, respectively (see Methods section).

The sign of the spectral function is determined by the denominator of Eq. (4), which is connected to all possible scattering mechanisms involving the emission or absorption of phonons. Typically, for conventional semiconductors, the Eliashberg function is positive at the valence band maximum (VBM) and negative at the conduction band minimum (CBM).[42,43] These opposite trends lead to the usual reduction of the band gap with temperature. Therefore, they provide a clear tool to investigate the anomalies induced by the electron-phonon interaction.

In Fig. (3-a), we show the Eliashberg function for the CBM and VBM states. It behaves as in conventional semiconductors for high frequency optical modes. However, in the AR they present opposite trends. By defining the band-edge Eliashberg function, F_g=F_{CBM}−F_{VBM}, we see that two very intense positive peaks appear in the AR. They are responsible for the positive slope in $E_{gap}(T)$ as one can inferred directly from Eq. (5) by identifying the

positive sign of the integral. Indeed, the AR is located in the low energy part of the phonon spectrum and, therefore, it is always weighted by the Bose distribution more than all other modes. Thus, we have the confirmation that the same phonon modes are responsible for both the harmonic and anharmonic anomalous gap correction.

The BP phonon dispersion shown in Fig. (3-b) allow us to further inspect the origin of the g^2F_n peaks. A careful analysis of the band-edge g^2F_n projected on each vibrational mode, shown in Fig. (3-c), clearly indicates that the peak around 146 cm^{-1} arises from the TA and TO modes. TA providing the most intense contribution. It should be noticed that the TA and TO modes have been previously[21] identified as the main sources for the anomalous band-gap temperature dependence (with TA being the predominant) in CuBr and $AgGaS_2$. This is consistent with our fully *ab-initio* results based on MBPT.

As we already observed in the LTE contribution analysis, the electron-phonon coupling related to the anomaly arises due to large phonon vibration amplitudes around the equilibrium position that are favored by the particular crystal structure of BP. Note that the mode B_{1g} does not contribute in the origin of the anomaly as its electron-phonon coupling is very weak in the anomalous region. These results confirm the predictions based on the superficial potential plots shown in Fig. (2-h). For completeness, in Fig. (3-d), we show g^2F_n for high frequency optical modes. From there we note that peak around 342 cm^{-1} stems from the coupling with the mode A_g^1. In addition, the origin of the high frequency peak is traced back and related mainly to the infrared active B_{2u} and the Raman active A_g^2 modes. This results are in agreement with a recent work in which the electron-phonon coupling in BP is assessed by means of group theory.[27]

In summary, by means of *ab-initio* calculations, we have shown that black phosphorus presents an anomalous band gap temperature dependence that arises due to electron-phonon coupling with acoustic and low-frequency transverse optical mode that also cause a negative pressure coefficient. The nature of the electron-phonon coupling is traced back to the large-amplitude atomic vibrations which are favored by the particular BP layered structure.

Our results spotlight the importance of both harmonic and lattice thermal expansion contributions on determining the band-gap thermal dependence. We also put in evidence the direct correlation between harmonic and anharmonic effects that can be used as fingerprints to identify thermal anomalies in other semiconductors.

2 Methods

The harmonic (constant volume) contribution to the temperature dependence of the electronic states is described within the Many-Body perturbation theory (MBPT) framework. In MBPT, the electron-phonon interaction is treated perturbatively and composed by a first and a second order Taylor expansion in the nuclear displacement,[33,34] which are commonly known as the Fan and Debye-Waller (DB) terms, respectively. The interacting Green's function, whose poles define the quasiparticle excitations, can be written as

$$G_{n\mathbf{k}}(\omega, T) = [\omega - \epsilon_{n\mathbf{k}} - \Sigma^{Fan}_{n\mathbf{k}}(\omega, T) - \Sigma^{DW}_{n\mathbf{k}}(T)]^{-1}, \tag{6}$$

where $\epsilon_{n\mathbf{k}}$ is the ground-state frozen atoms eigenenergies, obtained from plane-wave DFT.[44] Σ^{Fan} is the Fan contribution[45]

$$\Sigma^{Fan}_{n\mathbf{k}}(i\omega, T) = \sum_{n'\mathbf{q}\lambda} \frac{|g^{\mathbf{q}\lambda}_{nn'\mathbf{k}}|^2}{N} \Big[\frac{N_{\mathbf{q}\lambda}(T) + 1 - f_{n'\mathbf{k-q}}}{i\omega - \epsilon_{n'\mathbf{k-q}} - \omega_{\mathbf{q}\lambda}} + \frac{N_{\mathbf{q}\lambda}(T) + f_{n'\mathbf{k-q}}}{i\omega - \epsilon_{n'\mathbf{k-q}} + \omega_{\mathbf{q}\lambda}} \Big], \tag{7}$$

and Σ^{DW} is the Debye-Waller term

$$\Sigma^{DW}_{n\mathbf{k}}(T) = -\frac{1}{2} \sum_{n'\mathbf{q}\lambda} \frac{\Lambda^{\mathbf{q}\lambda}_{nn'\mathbf{k}}}{N} \Big[\frac{2N_{\mathbf{q}\lambda}(T) + 1}{\epsilon_{n\mathbf{k}} - \epsilon_{n'\mathbf{k}}} \Big]. \tag{8}$$

Here $N_{\mathbf{q}\lambda}$, $f_{n'\mathbf{k-q}}$ represent the Bose-Einstein and Fermi-Dirac distribution functions, while $\omega_{\mathbf{q}\lambda}$ and N are the phonon frequencies and number of $\mathbf{q}$ points taken randomly in the Brillouin zone. The electron-phonon matrix elements $g^{\mathbf{q}\lambda}_{nn'\mathbf{k}}$, which represent the probability amplitude

for an electron to be scattered with emission or absorption of phonons is given by [46]

$$g^{\mathbf{q}\lambda}_{nn'\mathbf{k}} = \sum_{s\alpha}[2M_s\omega_{\mathbf{q}\lambda}]^{-1/2}e^{i\mathbf{q}.\tau_s}\langle n'\mathbf{k\text{-}q}|\frac{\partial V_{scf}(\mathbf{r})}{\partial R_{s\alpha}}|n\mathbf{k}\rangle\xi_\alpha(\mathbf{q}\lambda|s), \tag{9}$$

where, M_s is the atomic mass, τ_s is the position of the atomic displacement in the unit cell and $\xi_\alpha(\mathbf{q}\lambda|s)$ are the components of the phonon polarization vectors. $V_{scf}(r)$ is the self-consistent DFT ionic potential. $\Lambda^{\mathbf{q}\lambda}_{nn'\mathbf{k}}$ are the second-order electron-phonon matrix elements which were calculated within the rigid-ion approximation.[34,46] A detailed discussion and derivation of the electron-phonon matrix elements, including $\Lambda^{\mathbf{q}\lambda}_{nn'\mathbf{k}}$ can be found elsewhere.[33,34]

By assuming the quasiparticle approximation (QPA) to expand in first-order the self-energy frequency dependence around the bare energies, one can write the non-adiabatic temperature dependent quasiparticle energy corrections as [47]

$$\Delta E_{n\mathbf{k}}(T)\big|_{har} = E_{n\mathbf{k}}(T) - \epsilon_{n\mathbf{k}} \approx Z_{n\mathbf{k}}(T)[\Sigma^{Fan}_{n\mathbf{k}}(\epsilon_{n\mathbf{k}},T) + \Sigma^{DW}_{n\mathbf{k}}(T)], \tag{10}$$

with the renormalization factor $Z_{n\mathbf{k}}(T)=\big[1\text{-}\frac{\partial\Re\Sigma^{Fan}_{n\mathbf{k}}(\omega)}{\partial\omega}\big|_{\omega=\epsilon_{n\mathbf{k}}}\big]^{-1}$. Given that the Fan self-energy term is a complex function, it provides both an energy renormalization shift and an intrinsic quasiparticle lifetime. It is worth to mention that the MBPT formalism presented here represents the dynamical extension of the Heine-Allen-Cardona approach [42] which is naturally recovered from eq. (7) by assuming $|\epsilon_{n\mathbf{k}} - \epsilon_{n'\mathbf{k\text{-}q}}| \gg \omega_{\mathbf{q}\lambda}$ (the *adiabatic* limit) and $\omega \approx \epsilon_{n\mathbf{k}}$ (the *on-the-mass-shell* limit). Thus, the adiabatic corrections can be written as

$$\Delta E_{n\mathbf{k}}(T)\big|^{adiab}_{har} \approx \Sigma^{Fan}_{n\mathbf{k}}(\epsilon_{n\mathbf{k}},T) + \Sigma^{DW}_{n\mathbf{k}}(T) = \int d\omega g^2 F_{n\mathbf{k}}(\omega)[N_{\mathbf{q}\lambda}(\omega,T) + \frac{1}{2}]. \tag{11}$$

The ground-state charge density and electronic states, necessary to evaluated Eq. (10), were obtained by performing plane-wave density functional theory (DFT) using the Perdew-Burke-Ernzerhof (PBE) exchange-correlation functional currently implemented in the Quantum-Espresso code. [44] Norm-conserving pseudopotentials with 3s3p core-states were adopted. The

Brillouin zone was mapped using 6×8×3 k-sampling with 80 Ry kinetic energy cut-off. The electron-phonon matrix elements necessary to compute the Fan and Debye-Waller self-energies, Eq. (7) and (8), were obtained within density functional perturbation theory (DFPT). In addition, the self-energies were evaluated with 400 electronic bands and 240 random **q**-points for the phonon momentum. These parameters were chosen after a careful convergence tests on the spectral function. The curves showing the convergence as a function of the electronic bands and **q**-points can be found in the supporting information.

The phonon frequencies dependence on volume (anharmonic contribution) is studied by means of the quasiharmonic approximation. Within this formalism, the equilibrium volume of a crystal for any temperature T, at a constant pressure, can be evaluated by minimizing the Helmholtz free energy function with respect the volume,[35,48]

$$F(\{V_i\},T) = E(\{V_i\}) + \sum_{\mathbf{q}\lambda} \frac{\hbar\omega_{\mathbf{q}\lambda}(\{V_i\})}{2} + k_B T \sum_{\mathbf{q}\lambda} \ln(1 - \exp[-\frac{\hbar\omega_{\mathbf{q}\lambda}(\{V_i\})}{k_B T}]), \tag{12}$$

where the function $E(V_i)$ is the ground-state energy, obtained from DFT calculations by applying uniaxial strain that varies by ± 2% at each crystallographic direction. Once the Helmholtz function is evaluated at different volumes, the data is fitted with the third-order Birch-Murnaghan equation of state. The linear thermal expansion coefficients of the cell are calculated as

$$\alpha_i(T) = \frac{1}{a_i(T)} \frac{da_i(T)}{dT}. \tag{13}$$

For the anharmonic contributions and energy gap pressure dependence, Van der Waals corrections were taken into account within the vdW-DF approach for the exchange-correlation functional. This was done in order to open the electronic gap and avoid the metal transition of the structure during the volume change. The anharmonic properties of the system were computed using the Phonopy package.[49] To this aim, a 2×2×2 supercell was constructed. Evaluating the Grüneisen parameters required to remove the system from the equilibrium volume, by changing the the lattice parameter by ± 0.35 %

Acknowledgement

CEPV acknowledges the financial support from the Brazilian agency FAPESP grant number 2015/14899-0 and 2012/24227-1. AM acknowledges the funding received from the Futuro in Ricerca grant No. RBFR12SW0J of the Italian Ministry of Education, University and Research MIUR, the European Union project MaX Materials design at the eXascale H2020-EINFRA-2015-1, Grant agreement n. 676598 and Nanoscience Foundries and Fine Analysis - Europe H2020-INFRAIA-2014-2015, Grant agreement n. 654360. A. R. R. acknowledges support from ICTP-SAIRF (FAPESP project 2011/11973-4) and the ICTP-Simons Foundation Associate Scheme. This work uses the computational resources from GRID-UNESP and CENAPAD/SP.

Supporting Information Available

Convergence test related to the temperature dependent electronic states; lattice constant as a function of temperature; lattice thermal expansion as a function of T. This material is available free of charge via the Internet at `http://pubs.acs.org/`.

References

(1) Wang, X.; Jones, A. M.; Tran, K. L. S. V.; Jia, Y.; Zhao, H.; Wang, H.; Yang, L.; Xu, X.; Xia, F. *Nat. Nanotech.* **2015**, *10*, 517–521.

(2) Xia, F.; Wang, H.; Jia, Y. *Nat. Commun.* **2015**, *5*, 4458.

(3) Ling, X.; Wang, H.; Huang, S.; Xia, F.; Dresselhaus, M. S. *Proc. Natl. Acad. Sci* **2015**, *112*, 201416581.

(4) Luo, Z.; Maassen, J.; Deng, Y.; Du, Y.; Garrelts, R. P.; Lundstrom, M. S.; Ye, P. D.; Xu, X. *Nat. Commun.* **2015**, *6*, 8572.

(5) Tran, V.; Soklaski, R.; Liang, Y.; Yang, L. *Phys. Rev. B* **2014**, *89*, 235319.

(6) Li, L.; Yu, Y.; Ye, G. J.; Ge, Q.; Ou, X.; Wu, H.; Feng, D.; Chen, X. H.; Zhang, Y. *Nat. Nanotech.* **2014**, *9*, 372–377.

(7) Yuan, H. et al. *Nat. Nanotech.* **2015**, *10*, 707–713.

(8) Qin, G.; Yan, Q.-B.; Qin, Z.; Yue, S.-Y.; Cui, H.-J.; Zheng, Q.-R.; Su, G. *Sci. Rep.* **2014**, *4*, 6949.

(9) Fei, R.; Faghaninia, A.; Soklaski, R.; Yan, J.-A.; Lo, C.; Yang, L. *Nano Lett.* **2014**, *14*, 6393–6399.

(10) Cardona, M.; Thewalt, M. L. W. *Rev. Mod. Phys.* **2005**, *77*, 1173.

(11) Varshni, Y. P. *Physica* **1967**, *34*, 149–154.

(12) Lefebvre, J.; Finnie, P.; Homma, Y. *Phys. Rev. B* **2004**, *70*, 045419.

(13) Bhosale, J.; Ramdas, A. K.; Burger, A.; Muñoz, A.; Romero, A. H.; Cardona, M.; Lauck, R.; Kremer, R. K. *Phys. Rev. B* **2012**, *86*, 195208.

(14) Yu, C.; Chen, Z.; Wang, J. J.; Pfenninger, W.; Vockic, N.; Kenney, J. T.; Shum, K. *J. Appl. Phys.* **2011**, *110*, 063526.

(15) Gobel, A.; Ruf, T.; Cardona, M.; Lin, C. T.; Wrzesinski, J.; Steube, M.; Reimann, K.; Merle, J.-C.; Joucla, M. *Phys. Rev. B* **1998**, *57*, 15183.

(16) Tauber, R. N.; Machonis, A. A.; Cadoff, I. B. *Jour. Appl. Phys.* **1966**, *37*, 4855.

(17) Gibbs, Z. M.; Kim, H.; Wang, H.; White, R. L.; Kaviany, F. D. M.; Snyder, G. J. *Appl. Phys. Lett.* **2013**, *103*, 262109.

(18) Tsang, Y. W.; Cohen, M. L. *Phys. Rev. B* **1971**, *3*, 1254.

(19) Baleva, M.; Georgiev, T.; Lashkarev, G. *J. Phys.: Condens. Matter* **1990**, *1*, 2935–2940.

(20) Hauschild, R.; Priller, H.; Decker, M.; Brückner, J.; Kalt, H.; Klingshirn, C. *phys. stat. sol. (c)* **2006**, *3*, 976–979.

(21) Cardona, M.; Kremer, R. K. *Thin Solid Films* **2014**, *571*, 680–683.

(22) Baba, M.; Nakamura, Y.; Shibata, K.; Morita, A. *Jpn. J. Appl. Phys.* **1991**, *30*, L1178.

(23) Morita, A. *Appl. Phys. A* **1986**, *39*, 227–242.

(24) Surrente, A.; Mitioglu, A. A.; Galkowski, K.; Tabis, W.; Maude, D. K.; Plochocka, P. *Phys. Rev. B* **2016**, *93*, 121405(R).

(25) Ribeiro, H. B.; Villegas, C. E. P.; Bahamon, D. A.; Muraca, D.; Castro-Neto, A. H.; de Souza, E. A. T.; Rocha, A. R.; Pimenta, M. A.; de Matos, C. J. S. *Nat. Comm.* **2016**, *7*, 12191.

(26) Ling, X.; Liang, L.; Huang, S.; Puretzky, A. A.; Geohegan, D. B.; Sumpter, B. G.; Kong, J.; Meunier, V.; Dresselhaus, M. S. *Nano Lett.* **2015**, *15*, 4080–4088.

(27) Ling, X. et al. *Nano Lett.* **2016**, *16*, 2260–2267.

(28) Barrera, G. D.; Bruno, J. A. O.; Barron, T. H. K.; Allan, N. L. *J. Phys. Condens. Matter* **2005**, *17*, R127–R252.

(29) $\Delta E_n\big|_{har}$ and $\Delta E_n\big|_{LTE}$ are approximated as both neglect higher order corrections. Here we assume that, as far as the electron-phonon channel is concerned, the Migdal's theorem holds and we can safely stick to the harmonic description. For the lattice expansion term, based on the quasi harmonic approximation, its accuracy is assumed for temperatures bellow $\Theta_D{=}h\nu_D/k_B = 281.72$K. Here $\nu_D{=}$ 5.85 THz, was estimated as the value of the highest frequency normal mode.

(30) Cannuccia, E.; Marini, A. *Phys. Rev. Lett.* **2011**, *107*, 255501.

(31) Delaire, O.; Ma, J.; Marty, K.; May, A. F.; McGuire, M. A.; Du, M.-H.; Singh, D. J.; Podlesnyak, A.; Ehlers, G.; Lumsden, M. D.; Sales, B. C. *Nat. Mater.* **2011**, *10*, 614.

(32) Božin, E. S.; Malliakas, C. D.; Souvatzis, P.; Proffen, T.; Spaldin, N. A.; Kanatzidis, M. G.; Billinge, S. J. L. *Science* **2010**, *630*, 1660–1663.

(33) Marini, A.; Poncé, S.; Gonze, X. *Phys. Rev. B.* **2015**, *91*, 224310.

(34) Poncé, S.; Antonius, G.; Gillet, Y.; Boulanger, P.; Janssen, J. L.; Marini, A.; Côté, M.; Gonze, X. *Phys. Rev. B.* **2014**, *90*, 214304.

(35) Dove, M. T. *Introduction to lattice dynamics*; Cambridge university press, 1993.

(36) Kaneta, C.; Yoshida, H. K.; Morita, A. *J. Phys. Soc. Jpn.* **1986**, *55*, 1213–1223.

(37) Rudenko, A. N.; Katsnelson, M. I. *Phys. Rev. B* **2014**, *89*, 201408(R).

(38) Riedner, R. J.; Srinivasa, S. R.; Cartz, L.; Worlton, T. G.; Klinger, R.; Beyerlein, R. *AIP Conf. Proc* **1974**, *17*, 8.

(39) Akahama, Y.; Kawamura, H. *physica status solidi (b)* **2001**, *223*, 349–353.

(40) Mounet, N.; Marzari, N. *Phys. Rev. B* **2005**, *71*, 205214.

(41) The Grüneisen parameter is linked to other thermodynamic observables through the relation $\gamma = \beta V/C_V\chi$, where C_V is the heat capacity and $\gamma = \sum_\lambda \gamma_\lambda C_\lambda / \sum_\lambda C_\lambda$, is defined as the weighted partial contribution for each mode λ. Similarly, C_λ is the heat capacity contribution of each phonon mode. Given that χ, V, $C_V > 0$ then, negative γ implies $\beta < 0$ which means a particular material should contracts as the temperature increases.

(42) Allen, P. B.; Cardona, M. *Phys. Rev. B* **1983**, *27*, 4760.

(43) Lautenschlager, P.; Allen, P. B.; Cardona, M. *Phys. Rev. B* **1985**, *31*, 2163.

(44) Giannozzi, P. et al. *J. Phys. Condens. Matter* **2009**, *21*, 395502.

(45) Cannuccia, E. *Giant Polaronic Effects in Polymers: Breakdown of the Quasiparticle Picture*; PhD thesis, Rome Tor Vergata University, 2011.

(46) Poncé, S.; Antonius, G.; Boulanger, P.; Cannuccia, E.; Marini, A.; Côté, M.; Gonze, X. *Comp. Mat. Sc.* **2014**, *83*, 341–348.

(47) Marini, A.; Hogan, C.; Grüning, M.; Varsano, D. *Comp. Phys. Commun.* **2009**, *180*, 1392.

(48) Togo, A.; Chaput, L.; Tanaka, I.; Hug, G. *Phys. Rev. B* **2010**, *81*, 174301.

(49) Togo, A.; Tanaka, I. *Scr. Mater.* **2015**, *108*, 1–5.